Method to quantify the electrical efficiency of a ns-DBD plasma actuator

Francesco Avallone[1,*] and Giuseppe Correale[1]

[1]Department of Aerospace Engineering, Delft University of Technology, Delft, The Netherlands
[*]corresponding author: f.avallone@tudelft.nl

Abstract An experimental investigation was conducted on the effective efficiency of a nanosecond Dielectric Barrier Discharge (ns-DBD) plasma actuator. Back-current shunt technique and infrared thermography measurements were carried out at the same time on an upside-down flat plate in a quiescent environment. The only investigated parameter was thickness of the dielectric barrier. Voltage amplitude and frequency of discharge were kept constant at maximum values allowable by the used power generator, i.e. 10k Volt and 10k Hz respectively. The selected material for the dielectric barrier was Makrolon® because of its well know thermal and dielectric propriety. Energy input was calculated as difference between the pulse voltage given and the one reflected back into the system via back current shunt technique. Ideal power flux obtained if all the input energy was converted to heat is then calculated. The actual power flux was obtained by solving an IHTP (Inverse Heat Transfer Problem) once the transient temperature distribution on the surface of the dielectric barrier was measured by means of IR thermography. The ratio between these two values represents a quantification of electrical efficiency of an ns-DBD plasma actuator. Results prove the high performances of ns-DBD plasma actuator in the respect of energy deposition and that the efficiency depends on the thickness of the barrier.
Keywords: Electrical efficiency, ns-DBD plasma actuator, IR thermography

1 Introduction

The capability to manipulate a flow to behave differently from what it naturally would is the basic definition of flow control. Among the different kinds of flow control techniques [1] the unsteady reactive ones, that use periodic excitations to manipulate flow instabilities [2, 3], have the potential to overcome any other flow control technique in terms of efficiency and effectiveness [4]. Several theoretical, experimental and numerical investigations have proven DBD plasma actuators [5, 6] to be effective means of reactive flow control, capable of manipulating the natural stability of a flow [7, 8, 9, 10, 11]. However, from commercial and environmental points of view a technology is not only evaluated for its effectiveness but also for its efficiency. In order to do so, it is of primary importance to identify the stages of power-flow through which energy passes. According to Kriegseis et al. [12] a DBD power-flow is divided in three stages, each suffering of energy losses. The first stage is related to the device itself, the second to the physical mechanism of flow control (different for different kinds of plasma actuators) and the third one related to the flow control task to be achieved. However, only at the first stage efficiency can be regarded as a univocally defined real non-dimensional coefficient that ranges between 0 and 1 [12]. Nevertheless, few example are found in literature aimed to qualify and quantify the second [13, 14, 15] and the third stage [16] as well. This work focuses on the first stage (called electrical efficiency), i.e. the efficiency of energy deposition within the discharge volume of a plasma actuator. More in particular, the nanosecond plasma actuators is investigated. Few attempts are found in literature to do so for the ac version of DBDs [17, 18, 19]. General observation is that the power drained from an ac-DBD is dependent on the load of the system itself, which is divided into two parts: one purely passive dependent on the actuator construction characteristics (geometry, material, etc.) and the other one discharge dependent, which is function of the shape of the driving high voltage signal. Electrical efficiency is therefore the ratio between the power input and the power drained. Having ac-DBDs their actuation mechanism relying on electromagnetic forces generated between the electrodes [20, 21], internal losses of energy, i.e. within the dielectric barrier, are relatively not affecting the control authority of these devices. Moreover, such losses are of difficult quantification and neglected most of the times. Differently, for the case of ns-DBDs which actuation mechanism relies on a thermal effect [22], quantification of the energy losses within the barrier is of primary importance in order to define the efficiency of energy deposition within the discharge volume. In this respect, internal losses are not just dependent on geometrical constructive characteristics [23, 24] but also on thermal properties of the dielectric material used as barrier ([25] under review). Therefore, for a given volumetric resistivity and geometry of

actuator, during the discharge period some energy flows throughout the barrier and gets lost or stored within the barrier in a sort of "capacitance" effect between electrodes. This happens on the time scales between the one of the discharge (nanosecond [23]) and the one of the plasma (microsecond [22]), and it represents the first part of the energy losses. On the time scale of the residual heat increase (milliseconds [11, 26]), heat generated by a discharge is conducted through the barrier and diffused internally. Due to the different time scales at which such losses happen, the first type of losses can be neglected. Summarising, the energy internally lost can be approximated to the residual heat that flows away through the barrier and does not get injected into the discharge volume, so affecting directly the control authority of ns-DBDs. In this paper temperature surface of the barrier and its time evolution are experimentally investigated. Experimental data are then used to compute power input. At the same time, measurements of actual "net energy input" in the actuator system is carried out via back-current shunt technique [11, 25]. The ratio between the power input found numerically and total power input calculated by shunt measurements gives, with good approximation, the electrical efficiency of a ns-DBD plasma actuator.

2 Experimental Setup

An experimental campaign was carried out in order to quantify the electrical efficiency [12] of a ns-DBD plasma actuator. Moreover, the influence of the barrier thickness was investigated. Time-locked infrared measurements were used to measure the time evolution of the surface temperature of the barrier of a ns-DBD actuator. Simultaneously, back current shunt technique was employed to measure the net electrical energy input. A one-dimensional heat equation in the direction normal to the surface is used to calculate the actual power flux produced by the discharge.

2.1 Model and plasma actuator

A nanosecond Dielectric Barrier Discharge plasma actuator was constructed using two electrodes made out of adhesive copper tape, separated by a dielectric barrier. The tested plasma actuator was flush mounted on a upside-down flat plate (in order to minimize the effect of natural convection) placed in a still air environment. Electrodes were placed such to have no gap, i.e. zero horizontal distance between each other. A sketch of plasma actuator layout together with the reference system used is given in figure 1.

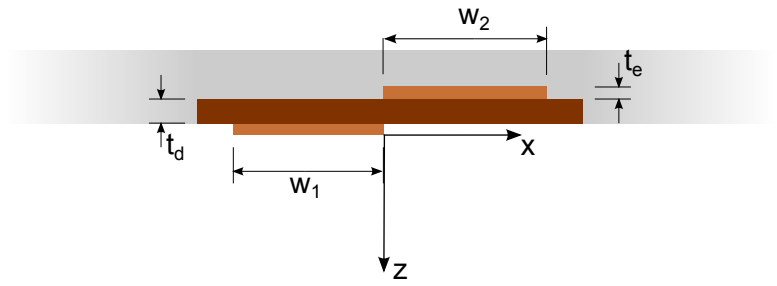

Fig. 1 Sketch of ns-DBD plasma actuator layout and Cartesian coordinate system.

The material selected for the barrier was Makrolon® given its well-known thermal and electrical proprieties. Three thicknesses (t_d) were investigated, i.e. 1, 1.5 and 2 mm. Length of the copper electrodes was 100*mm*, width 5*mm* and the electrode overlap was zero in all the tested cases. The thickness of the self-adhesive electrodes was 0.06*mm* with additional 0.04*mm* of adhesive. An overview of the geometrical proprieties of the tested actuators is listed in table 1.

2.2 Back-current shunt

Power measurements were done via the back-current shunt technique in order to calculate energy associated with a single pulse. A shunt monitor resistor was built using 16 resistors, of 3.2Ω each, placed in parallel,

Table 1 Actuator parameters

Symbol	Description	Value	Units
W_1	Covered electrode width	5	*mm*
W_2	Exposed electrode width	5	*mm*
t_d	Dielectric thickness	$1/1.5/2$	*mm*
g_e	Gap between electrodes	≈ 0	*mm*
t_e	Electrode thickness	0.1	*mm*
l	Spanwise actuator length	100	*mm*
V_{pp}	Pulse voltage	10	*kV*
	Electrode material	Copper	N/A
	Dielectric material	Makrolon®	N/A

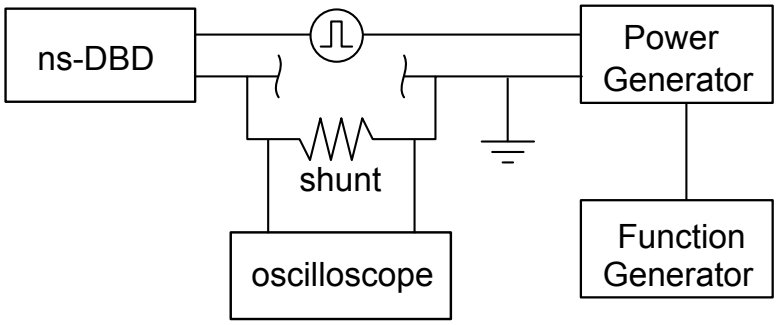

Fig. 2 Electrical setup of back current shunt technique.

resulting in an overall shunt resistance of 0.2Ω. In figure 2 an electrical scheme of the set-up is given for reference.

The shunt resistor was placed in the middle of the ground electrode of a $20m$ long high voltage coaxial cable (type RG-217). This high voltage cable was used to deliver the high voltage nanosecond pulse from a power generator to the tested plasma actuator. The shunt resistor was calibrated by applying a known signal of $5V$ from an Arbitrary Function Generator (Tektronics AFG3252) and measuring the voltage across the shunt directly with a digital oscilloscope of $1GHz$ which was set to impedance such to match the one of the high voltage cable, i.e. 50Ω. For the actual measurements a $20dB$ signal attenuator was used in order to protect the oscilloscope from voltage overload. The attenuation constant of the shunt resistor K_{sh} is theoretically calculated to be 250 using:

$$K_{sh} = \frac{Z}{R_{sh}} \tag{1}$$

where Z is the impedance of the high voltage cable and R_{sh} is the total resistance of the shunt respectively 50 and 0.2Ω. The calibration process yielded a K_{sh} of 253.97, value very close to the one calculated. Measurements of pulse energy were performed by measuring the voltage across the shunt resistor directly with an oscilloscope. In figure 3 a typical discharged pulse, as measured across the shunt, is presented.

The voltage signal presents two peaks, the first one represents the total electrical energy input given by the power generator (E_{in}). Given the shortness of the discharge, according to transmission line theory [27] energy contained into each single nanosecond pulse can be calculated from equation 2:

$$E_{in} = \int P_{in} dt = \int V_{in} I_{in} dt = \int \frac{V_{in}^2}{Z} dt \tag{2}$$

where V_{in} and I_{in} are respectively the voltage and the current input, and Z is the impedance of the high

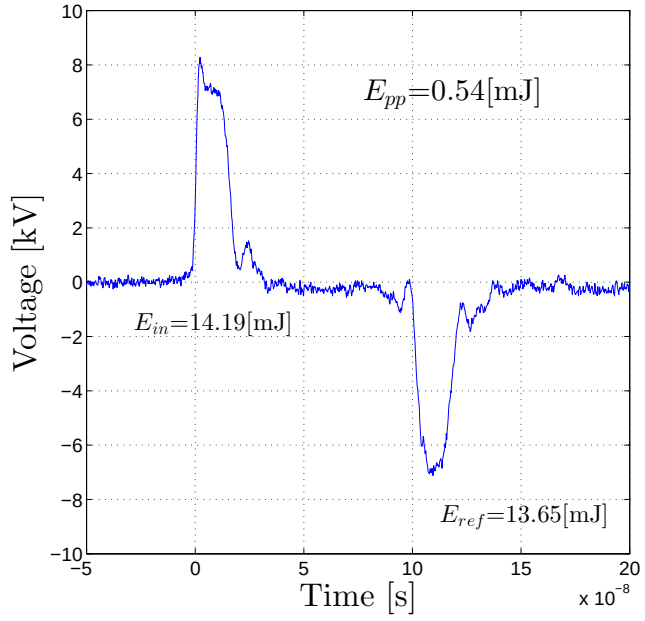

Fig. 3 Typical voltage signal calculated through the back-current shunt measurements.

voltage cable. It is noted that V_{in} was not directly measured but calculated from the voltage developed across the shunt V_{sh} according to equation 3:

$$V_{in} = V_{in} \times K_{sh} \tag{3}$$

The second peak in figure 3 represents the energy reflected back within the system (E_{ref}). The actual energy input, i.e. the net electrical energy transferred to the flow and lost internally by a plasma actuator, is calculated as the difference between the absolute value of the energy given by the first peak of the voltage signals (E_{in}, the energy input) and the second peak of the voltage signals (E_{ref} the energy reflected back into the high voltage cable), according to equation 4:

$$E_{pp} = E_{in} - E_{ref} \tag{4}$$

where E_{pp} is the net electrical energy per pulse deposited within the discharge volume and lost internally by the plasma actuator itself.

2.3 Infrared thermography

Infrared thermography [28] was used to map the transient temperature distribution of the dielectric barrier surface induced by a nanosecond high voltage pulsed discharge. The measurements were performed using a *CEDIP Titanium* 530*L IR* system. The camera has a Mercury Cadmium Telluride (MCT) quantum detector array of 320×256 pixels and a spectral response of $7.7-9.3\mu m$. The sensor is cooled to $77K$ by a Stirling cycle and has an NETD (Noise Equivalent Temperature Difference) of $25mK$. The integration time of the camera was set to $400\mu s$, while the acquisition frame rate was $200Hz$. A germanium lens with $25mm$ focal length and 2.0 numerical aperture ($f_{\#}$) was employed to obtain a spatial resolution of approximately $1.6px/mm$. The camera was located on a traverse system and the tested ns-DBD actuator was imaged through a parabolic mirror in order to increase image magnification, as sketched in figure 4.

The IR acquisition system was calibrated using a black-body built in-house and the mirror was kept installed during the calibration process to correct for its transmissivity. The camera was oriented at an angle of

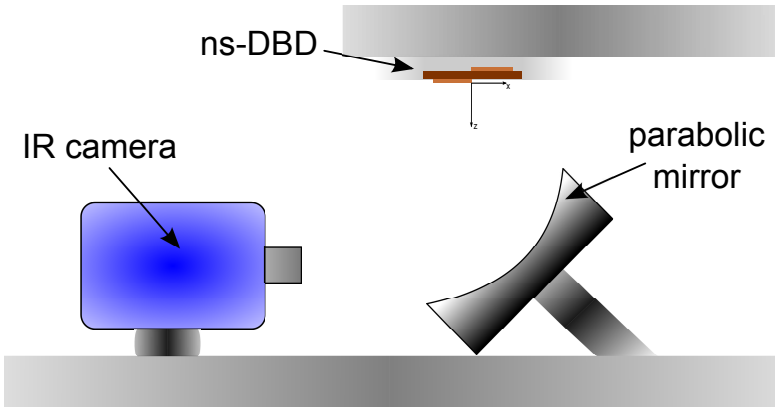

Fig. 4 Sketch IR set-up. Actuator dimensions are exaggerated for clarity.

approximately 10 degrees with respect to the mirror to prevent self-reflection. The model surface was set at an angle smaller than 50 degrees with respect to the camera sensor thus the emissivity could be regarded as constant and independent of the viewing angle [28]. The transient temperature acquisition started $400\mu s$ after the end of the discharge in order to reduce electromagnetic interferences induced by a nanosecond high voltage discharge and recorded for $100ms$.

2.4 Heat Transfer Data Reduction

The wall heat flux distribution is computed from the surface temperature signal by solving a one-dimensional Inverse Heat Transfer Problem (IHTP) based on the semi-infinite slab model coupled with a least square approach [29]. Starting from the temperature history measured by IR thermography, the heat flux (q) is evaluated by minimizing the difference between the computed temperature drop due to the heat conduction inside the model, obtained by solving the one-dimensional heat equation inside the body (eq. 5), and the measured experimental one (see figure 5 [30]). The optimization is performed by means of the Trust Region Reflective algorithm. The numerical temperature rise is computed by solving the heat equation inside the body with the boundary conditions as indicated in equations 5:

$$\begin{cases} k\nabla^2(T) = \rho c_p \frac{\partial T}{\partial t} \\ T(x_0,\ y_0,\ z,\ 0) = T_{wi} \\ k\ \frac{\partial T(x_0,\ y_0,\ z,\ t)}{\partial n}\Big|_s = q(t)\ \ and\ \ T(x_0,\ y_0,\ z\ \ \in F,\ t) = T_{wi} \end{cases} \tag{5}$$

In equation 5 (x_0, y_0) are the pixel coordinates in which the temperature is measured, S is the barrier surface exposed to the discharge while F is the opposite one.

In equation 5, k is the thermal conductivity, ρ is the density, c_p is the specific heat, T_{wi} is the initial temperature and q is the heat flux due to the discharge. The initial temperature distribution T_{wi} is known from the measurements and it is considered to be constant in the entire domain. The surface F is taken sufficiently deep in the model. A known temperature T_F is used as boundary condition at the wall not exposed to the discharge (F). The wall F is considered as isotherm so that $T(x_0,\ y_0,\ z\ \ \in F,\ t) = T_{wi}$. The assumption is assumed to be valid if the penetration depth ($d_p = 4\sqrt{\alpha t}$ where $\alpha = 1.4 \times 10^-7 m^2 s^-1$ is the material thermal diffusivity[31]) is smaller than the thickness of the material.

The heat transfer problem is solved using parabolic partial differential equations. The time integration is performed using a backward approach. The spatial discretization is made evaluating the convergence in the solution of the heat equation. The thickness of the material is set to be equal to the thickness of the discharge material. The discharge is modelled as a continuous and time-constant heat source acting for the given discharge time ($t_d \times n_{pulse}$).

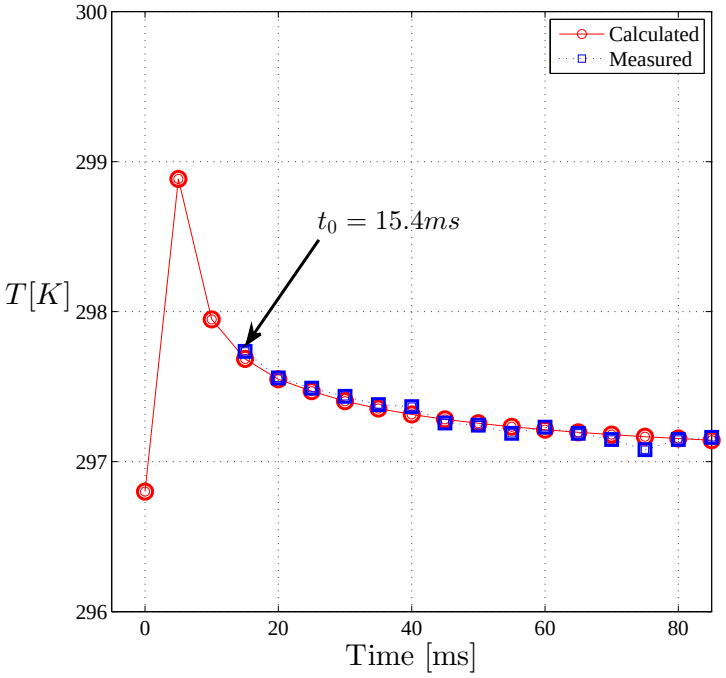

Fig. 5 Best fit between the experimental data and the solution of the heat equation 5. The investigated case corresponds to slab thickness of $1.5mm$. In the figure a black arrow indicates the initial instant time t_0 of measurements.

Table 2 Averaged energy input per pulse and per burst

thickness	1	1.5	2	Units [mm]
Averaged E_{pp}	1.5×10^{-3}	1.3×10^{-3}	7.14×10^{-4}	$[J]$
$E_{pp} \times 50p$	7.59×10^{-2}	6.61×10^{-2}	3.57×10^{-2}	$[J]$

At the end of the discharge, the heat flux is set equal to zero and the temperature of the surface exposed to the discharge drops due to heat conduction inside the material and natural convection. However, for the current analysis, the latter is considered negligible because of the upside-down configuration.

In order to visualize the actual size of the discharge, the temperature map is averaged along the length of the actuator (figure 6). The measured discharge size is about $2mm$. The same surface is considered for calculating the hypothetical power flux obtained if the 100% of the energy input (see table 3) was converted in heat.

3 Results

Back-current shunt technique is carried out and the values of the averaged energy input per pulse and per burst are given in table 2.

Infrared experiments and calculations are carried out in order to evaluate the electrical efficiency of a ns-DBD plasma actuator. With electrical efficiency it is meant the efficiency of the transformation from electrical energy to heat. Such transformation is of primary importance in the case of ns-DBDs since their physical actuation mechanism relies on a thermal effect [11, 22]. The method employed in this work is composed by three steps:

- IR termography is carried out in order to measure the transient temperature surface of the dielectric barrier and the extent of the surface exposed to the electrical discharge;

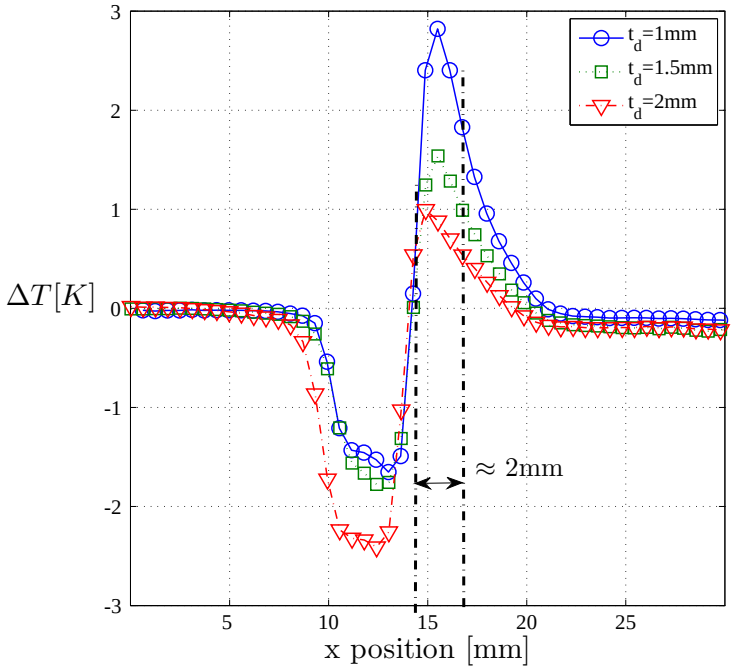

Fig. 6 Spanwise average of the temperature map at $t_0 = 15.4ms$

Table 3 Power flux computed and calculated from experiments

thickness	1	1.5	2	Units [mm]
measured	3.92×10^4	3.08×10^4	1.97×10^4	$[W/m^2]$
calculated	3.68×10^4	2.82×10^4	1.47×10^4	$[W/m^2]$

- Back-current shunt technique is employed to measure the "net electrical energy input", and then it is converted into power flux;
- A one dimensional IHTP is solved in order to compute the actual power flux output.

The ratio between the two power fluxes is considered to be the electrical efficiency of the tested ns-DBD plasma actuator. A characterization of the dielectric barrier thickness is performed as well, in order to evaluate the influence of the barrier thickness on the net electrical performance of a ns-DBD plasma actuator. In table 3, the measured and calculated power flux are presented for all the investigated cases.

As expected, the calculated values (representing only the actual energy deposited within the discharge volume) are smaller than the one calculated for the total energy input. Table 4 gives the uncertainty in the measurement of the total energy input corresponding to 0.44, 0.58 and 0.89% of the total energy input (see table 2) for thicknesses of 1, 1.5 and 2*mm*, respectively.

From tables 3 and 4 it can be observed that the values of the net energy input and of the RMS show a trend

Table 4 Uncertainty quantification

thickness	1	1.5	2	Units [mm]
RMS_{exp}	0.44	0.58	0.89	[%]
RMS_{calc}	10	12	14	[%]

Table 5 Electrical efficiency and losses.

thickness	1	1.5	2
η	0.94	0.92	0.75

related to the thickness of the barrier. This is due to the fact that the energy deposition is dependent on the geometrical, electrical and thermal propriety of the barrier [25, 32], i.e. the thicker is the barrier the smaller is the amount of energy deposited into the volume. In table 5 the values of energy loss and efficiency for the tested thicknesses are reported.

4 Conclusions

Results of a research about quantification of electrical efficiency of ns-DBD plasma actuators were presented in this paper. The proposed approach consists of three steps. The total electrical energy input is first measured via back-current shunt technique and converted into power flux based on the period of the discharge and the average dimension of the discharge region evaluated directly from the temperature data (see figure 6). Then the time resolved infrared measurements are carried out in order to measure the top layer temperature of the barrier. Afterwards, the measured transient surface temperature is fit to the temperature obtained by solving a one-dimensional heat equation in a direction normal to the surface, as done for ac-DBD plasma actuator [33]. Numerical results are obtained by assuming that the residual heat within the discharge volume induced by a pulsed nanosecond high voltage discharge is adjacent to the surface of the barrier. Moreover, having the tested sample placed on a flat plate flipped upside-down the expansion of the heated volume is limited by a stratification effect. In this case natural convection is limited and considered small with respect conduction. Therefore, as first approximation the heat transfer is modelled as conduction throughout the barrier. The code makes use of an initial guessed value of power flux given as input and via an iterative process it finds the value of power flux capable to give the temperature time evolution matching the one measured. However, calculations are to be considered conservative since the bust discharge is modelled as a time constant heat flux. With this method it was possible to calculate the actual power flux emitted by the heated volume. Moreover, the ideal power flux obtained if all the input energy was transformed into heat is calculated. The difference between these two values represents the internal losses of a ns-DBD plasma actuator and their ratio is a quantification of the electrical efficiency of ns-DBDs, as reported in table 5. It is found that for the case of smallest dielectric barrier thickness, i.e. for a barrier $1mm$ thick, an efficiency over the 90% is calculated. This means that about the 90% of the input energy is converted into heat, so contributing to the formation of the "hot spot" [11, 34] that delivers the actuation of the flow when immerse into a laminar separated shear layer. Such value is evaluated to be affected by en error of about to 20%. However, the level of efficiency and of uncertainty increases as the thickness of the barrier increases. Simple conclusions about the electrical efficiency of a ns-DBD plasma actuator can not be draw out at the current state of this research. In order to better characterize the electrical efficiency of a ns-DBD plasma actuator further research is required were a much higher number of sample are analysed. Moreover, it is of primary importance to increase number of variables and cases such as thicknesses investigated and different materials. Nevertheless, the goal of this paper was to present a method to quantify electrical efficiency. Such method requires the coupling of back-current shunt technique with infrared thermal acquisitions.

References

[1] M. Gad-El-Hak, *Flow Control: Passive, Active, and Reactive Flow Management*. 2000.
[2] A. Seifert, A. Darabi, and I. Wygnanski, "Delay of airfoil stall by periodic excitation," vol. 33, no. 4, pp. 691–698, 1996.
[3] D. Greenblatt and I. J. Wygnanski, "The control of flow separation by periodic excitation," *Progress in Aerospace Sciences*, vol. 36, no. 7, pp. 487 – 545, 2000.
[4] L. Cattafesta and M. Sheplak, "Actuators for active flow control," vol. 43, pp. 247–272, 2011.

[5] E. Moreau, "Airflow control by non-thermal plasma actuators," *Journal of Physics D: Applied Physics*, vol. 40, no. 3, pp. 605–636, 2007. Cited By (since 1996): 388.

[6] T. C. Corke, M. L. Post, and D. M. Orlov, "Single dielectric barrier discharge plasma enhanced aerodynamics: Physics, modeling and applications," *Experiments in Fluids*, vol. 46, no. 1, pp. 1–26, 2009. Cited By (since 1996): 50.

[7] S. Grundmann and C. Tropea, "Active cancellation of artificially introduced tollmien-schlichting waves using plasma actuators," vol. 44, no. 5, pp. 795–806, 2008.

[8] A. Duchmann, A. Reeh, R. Quadros, J. Kriegseis, and C. Tropea, "Linear stability analysis for manipulated boundary-layer flows using plasma actuators," vol. 18, pp. 153–158, 2010.

[9] M. Kotsonis, R. Giepman, S. Hulshoff, and L. Veldhuis, "Numerical study of the control of tollmien-schlichting waves using plasma actuators," vol. 51, no. 10, pp. 2353–2364, 2013.

[10] A. Duchmann, B. Simon, P. Magin, C. Tropea, and S. Grundmann, "In-flight transition delay with dbd plasma actuators," 2013.

[11] G. Correale, T. Michelis, D. Ragni, M. Kotsonis, and F. Scarano, "Nanosecond-pulsed plasma actuation in quiescent air and laminar boundary layer," *Journal of Physics D: Applied Physics*, vol. 47, no. 10, p. XX, 2014. cited By (since 1996)3.

[12] J. Kriegseis, B. Möller, S. Grundmann, and C. Tropea, "On performance and efficiency of dielectric barrier discharge plasma actuators for flow control applications," vol. 4, no. 3-4, pp. 125–131, 2012.

[13] A. Hoskinson, Hershkowitz, and D. Ashpis, "Force measurements of single and double barrier dbd plasma actuators in quiescent air," vol. 41, no. 24, 2008.

[14] J. Ferry and J. Rovey, "Thrust measurement of dielectric barrier discharge plasma actuators and power requirements for aerodynamic control," 2010.

[15] R. Giepman and M. Kotsonis, "On the mechanical efficiency of dielectric barrier discharge plasma actuators," vol. 98, no. 22, 2011.

[16] A. Seifert, "Evaluation criteria and performance comparison of actuators for bluff-body flow control," American Institute of Aeronautics and Astronautics Inc., 2014.

[17] J. Reece Roth and X. Dai, "Optimization of the aerodynamic plasma actuator as an electrohydrodynamic (ehd) electrical device," vol. 19, pp. 14604–14631, 2006.

[18] J. Kriegseis, B. Möller, S. Grundmann, and C. Tropea, "Capacitance and power consumption quantification of dielectric barrier discharge (dbd) plasma actuators," vol. 69, no. 4, pp. 302–312, 2011.

[19] J. Kriegseis, S. Grundmann, and C. Tropea, "Power consumption, discharge capacitance and light emission as measures for thrust production of dielectric barrier discharge plasma actuators," vol. 110, no. 1, 2011.

[20] C. Enloe, T. McLaughlin, R. VanDyken, K. Kachner, E. Jumper, and T. Corke, "Mechanisms and responses of a single dielectric barrier plasma actuator: Plasma morphology," *AIAA Journal*, vol. 42, no. 3, pp. 589–594, 2004.

[21] C. Enloe, T. McLaughlin, R. VanDyken, K. Kachner, E. Jumper, T. Corke, M. Post, and O. Haddad, "Mechanisms and responses of a single dielectric barrier plasma actuator: Geometric effects," *AIAA Journal*, vol. 42, no. 3, pp. 595–604, 2004.

[22] D. V. Roupassov, A. A. Nikipelov, M. M. Nudnova, and A. Y. Starikovskii, "Flow separation control by plasma actuator with nanosecond pulsed-periodic discharge," *AIAA Journal*, vol. 47, no. 1, pp. 168–185, 2009.

[23] D. Opaits, M. Shneider, and R. Miles, "Electrodynamic effects in nanosecond-pulse-sustained long dielectric-barrier-discharge plasma actuators," *Applied Physics Letters*, vol. 94, no. 6, p. xx, 2009. cited By (since 1996)8.

[24] R. Dawson and J. Little, "Characterization of nanosecond pulse driven dielectric barrier discharge plasma actuators for aerodynamic flow control," *Journal of Applied Physics*, vol. 113, no. 10, 2013.

[25] G. Correale, R. Winkel, and M. Kotsonis, "Energy deposition characteristics of ns-dbd plasma actuators: Influence of dielectric material," *Journal of Applied Physics*, 2015.

[26] J. Zheng, Z. Zhao, J. Li, Y. Cui, and B. Khoo, "Numerical simulation of nanosecond pulsed dielectric barrier discharge actuator in a quiescent flow," vol. 26, no. 3, 2014.

[27] L. N. Dworsky, *Modern Transmission Line Theory and Applications*. Krieger Publishing Company, 1980.
[28] G. Carlomagno and G. Cardone, "Infrared thermography for convective heat transfer measurements," *Experiments in Fluids*, vol. 49, no. 6, pp. 1187–1218, 2010.
[29] F. Avallone, C. Greco, F. Schrijer, and G. Cardone, "A low-computational-cost inverse heat transfer technique for convective heat transfer measurements in hypersonic flows," *Experiments in Fluids*, vol. 56, no. 4, 2015.
[30] F. Avallone, C. Greco, and D. Ekelschot, "Image resection and heat transfer measurements by ir thermography in hypersonic flows," *Quantitative InfraRed Thermography Journal*, vol. 10, no. 2, pp. 188–206, 2013.
[31] D. Schultz and T. Jones, "Heat-transfer measurements in short-duration hypersonic facilities.," *AGARDograph*, no. 165, 1973.
[32] R. Winkel, G. Correale, and M. Kotsonis, "Effect of dielectric material on thermal effect produced by ns-dbd plasma actuator," in *AIAA*, 2014.
[33] R. Joussot, D. Hong, H. Rabat, V. Boucinha, R. Weber-Rozenbaum, and A. Leroy-Chesneau, "Thermal characterization of a dbd plasma actuator: Dielectric temperature measurements using infrared thermography," 2010.
[34] T. Michelis, G. Correale, I. B. Popov, M. Kotsonis, D. Ragni, S. J. K. Hulshoff, and L. L. M. Veldhuis, "Disturbance introduced into a laminar boundary layer by a NS-DBD plasma actuator," in *51st AIAA Aerosp. Sci. Meet. Incl. New Horizons Forum Aerosp. Expo. 2013*, 2013.